JOURNAL OF GEOPHYSICAL RESEARCH, VOL. 95, NO. D10, PAGES 16,601–16,615, SEPTEMBER 20, 1990

Intercomparison and Interpretation of Climate Feedback Processes in 19 Atmospheric General Circulation Models

R. D. CESS,[1] G. L. POTTER,[2] J. P. BLANCHET,[3] G. J. BOER,[3] A. D. DEL GENIO,[4] M. DÉQUÉ,[5] V. DYMNIKOV,[6] V. GALIN,[6] W. L. GATES,[2] S. J. GHAN,[2] J. T. KIEHL,[7] A. A. LACIS,[4] H. LE TREUT,[8] Z.-X. LI,[8] X.-Z. LIANG,[9] B. J. MCAVANEY,[10] V. P. MELESHKO,[11] J. F. B. MITCHELL,[12] J.-J. MORCRETTE,[13] D. A. RANDALL,[14] L. RIKUS,[10] E. ROECKNER,[15] J. F. ROYER,[5] U. SCHLESE,[15] D. A. SHEININ,[11] A. SLINGO,[7] A. P. SOKOLOV,[11] K. E. TAYLOR,[2] W. M. WASHINGTON,[7] R. T. WETHERALD,[16] I. YAGAI,[17] AND M.-H. ZHANG[9]

The need to understand differences among general circulation model projections of CO_2-induced climatic change has motivated the present study, which provides an intercomparison and interpretation of climate feedback processes in 19 atmospheric general circulation models. This intercomparison uses sea surface temperature change as a surrogate for climate change. The interpretation of cloud-climate interactions is given special attention. A roughly threefold variation in one measure of global climate sensitivity is found among the 19 models. The important conclusion is that most of this variation is attributable to differences in the models' depiction of cloud feedback, a result that emphasizes the need for improvements in the treatment of clouds in these models if they are ultimately to be used as reliable climate predictors. It is further emphasized that cloud feedback is the consequence of all interacting physical and dynamical processes in a general circulation model. The result of these processes is to produce changes in temperature, moisture distribution, and clouds which are integrated into the radiative response termed cloud feedback.

1. INTRODUCTION

Projected increases in the concentration of atmospheric carbon dioxide and other greenhouse gases are expected to have an important impact on climate. The most comprehensive way to infer future climatic change associated with this perturbation of atmospheric composition is by means of three-dimensional general circulation models (GCMs). *Schlesinger and Mitchell* [1987] have, however, demonstrated that several existing GCMs simulate climate responses to increasing CO_2 that differ considerably. *Cess and Potter* [1988], following a suggestion by *Spelman and Manabe* [1984], indicate that differences in global-mean warming, as predicted by five GCMs, might be partially attributable to the GCMs' differing control climates. Nevertheless, after accounting for this possibility, there still appear to be significant differences in the geographical distributions of the simulated warmings. Furthermore, two recent investigations [*Mitchell et al.*, 1989; J. P. Blanchet, private communication, 1989] suggest the importance of other factors with regard to differences in global-mean warming.

An understanding of the reasons for these differences requires a systematic examination and intercomparison of the parameterizations and processes in different models. If a broad spectrum of modeling groups are to participate in such a GCM intercomparison, simplicity is a necessary condition. With this in mind, *Cess and Potter* [1988] proposed a procedure in which perturbations in sea surface temperature serve as a surrogate climate change for the purpose of both intercomparing and understanding climate feedback processes in atmospheric GCMs. They further illustrated that cloud feedback could readily be inferred by separately treating clear and overcast regions within a model.

The purpose of the present study is to use this approach to interpret and intercompare atmospheric climate feedback processes in 19 different GCMs, with particular emphasis on understanding the role of clouds. As emphasized by *Cess et al.* [1989], in an early summary of this intercomparison, cloud feedback is the cause of much of the intermodel differences in climate sensitivity. The important point here is not simply to illustrate differences among models but to understand why these differences occur. As will become evident, it is especially important to understand that some models produce similar climate sensitivities as a consequence of very different cloud feedback components that compensate to produce similar net feedbacks.

[1]State University of New York, Stony Brook.
[2]Lawrence Livermore National Laboratory, Livermore, California.
[3]Canadian Climate Centre, Downsview, Ontario, Canada.
[4]NASA Goddard Institute for Space Studies, New York.
[5]Direction de la Météorologie Nationale, Toulouse, France.
[6]USSR Academy of Sciences, Moscow.
[7]National Center for Atmospheric Research, Boulder, Colorado.
[8]Laboratoire de Météorologie Dynamique, Paris, France.
[9]Institute of Atmospheric Physics, Beijing, China.
[10]Bureau of Meteorology Research Centre, Melbourne, Australia.
[11]Main Geophysical Observatory, Leningrad, USSR.
[12]United Kingdom Meteorological Office, Bracknell, Berkshire, England.
[13]European Centre for Medium-Range Weather Forecasts, Reading, Berkshire, England.
[14]Colorado State University, Fort Collins.
[15]University of Hamburg, Hamburg, Germany.
[16]National Oceanic and Atmospheric Administration, Geophysical Fluid Dynamics Laboratory, Princeton, New Jersey.
[17]Meteorological Research Institute, Tsukuba, Japan.

Paper number 90JD01219.
0148-0227/90/90JD-01219$05.00

2. INTERCOMPARISON AND INTERPRETATION METHODOLOGY

Many facets of the climate system are not well understood, and thus the uncertainties in modeling atmospheric, cryospheric, and oceanic interactions are large. In evaluating the differences among models, attention has been focused here on atmospheric processes, because these uncertainties must be understood before others can be addressed. For simplicity, emphasis is placed solely on global-average quantities, and the conventional interpretation is adopted of climate change as a two-stage process: forcing and response [*Cess and Potter*, 1988]. This concept of global-average forcing and response has proven useful in earlier interpretations of cloud feedback. For example, by performing two GCM simulations for a doubling of atmospheric CO_2 concentration, one with computed clouds and the other with clouds that were invariant to the change in climate, *Wetherald and Manabe* [1988] have suggested that cloud feedback amplifies global warming by the factor 1.3. A somewhat larger amplification (1.8) is found from the study by *Hansen et al.* [1984], who used a one-dimensional climate model to evaluate climate feedback mechanisms within a different GCM. A further discussion of these results will be presented in section 6.

The global-mean direct radiative forcing G of the surface-atmosphere system is evaluated by holding all other climate parameters fixed. It is this quantity that induces the ensuing climate change, and physically, it represents a change in the net (solar plus infrared) radiative flux at the top of the atmosphere (TOA). For an increase in the CO_2 concentration of the atmosphere, to cite one example, G is the reduction in the emitted TOA infrared flux resulting solely from the CO_2 increase, and this reduction results in a heating of the surface-atmosphere system. The response process is the change in climate that is then necessary to restore the TOA radiation balance, such that

$$G = \Delta F - \Delta Q \tag{1}$$

where F and Q respectively denote the global-mean emitted infrared and net downward solar fluxes at the TOA. Thus ΔF and ΔQ represent the climate-change TOA responses to the direct radiative forcing G, and these are the quantities that are impacted by climate feedback mechanisms. Furthermore, the change in surface climate, expressed as the change in global-mean surface temperature ΔT_s, can be related to the direct radiative forcing G by

$$\Delta T_s = \lambda G \tag{2}$$

where λ is the climate sensitivity parameter

$$\lambda = (\Delta F/\Delta T_s - \Delta Q/\Delta T_s)^{-1} \tag{3}$$

An increase in λ thus represents an increased climate change due to a given climate forcing G.

A simple example illustrates the use of λ for evaluating feedback mechanisms. If only the basic temperature-radiation negative feedback exists, then climate change refers solely to temperature change, and there are no related changes in atmospheric composition, lapse rate, or surface albedo. Thus $\Delta Q/\Delta T_s = 0$, and to evaluate $\Delta F/\Delta T_s$ assume that $F = \varepsilon\sigma T_s^4$ [*Cess*, 1976], where σ is the Stefan-Boltzmann constant and ε is the emissivity of the surface-atmosphere system, which is constant in this case. It then follows that $\Delta F/\Delta T_s = 4F/T_s = 3.3$ W m^{-2} K^{-1} for conditions typical of Earth ($F = 240$ W m^{-2} and $T_s = 288$ K), so that in the absence of interactive feedback mechanisms

$$\lambda = 0.3 \text{ K m}^2 \text{ W}^{-1} \tag{4}$$

A well-known positive feedback mechanism is water vapor feedback [*Manabe and Wetherald*, 1967], in which a warmer atmosphere contains more water vapor, which as a greenhouse gas amplifies the initial warming. Climate models that contain this positive feedback typically give $\Delta F/\Delta T_s \simeq 2.2$ W m^{-2} K^{-1}. In addition, the increased water vapor increases the atmospheric absorption of solar radiation, and for a typical model this positive feedback yields $\Delta Q/\Delta T_s \simeq 0.2$ W m^{-2} K^{-1}. Thus with the inclusion of water vapor feedback the sensitivity parameter is increased from that given in (4) to

$$\lambda \simeq 0.5 \text{ K m}^2 \text{ W}^{-1} \tag{5}$$

Whereas water vapor feedback is straightforward to understand, cloud feedback is a far more complex phenomenon. There are several ways that clouds can produce feedback mechanisms. For example, if global cloud amount decreases because of climate warming, as occurred in simulations with the 19 GCMs we employed, then this decrease reduces the infrared greenhouse effect due to clouds. Thus as the Earth warms, it is able to emit infrared radiation more efficiently, moderating the global warming and so acting as a negative climate feedback mechanism. But there is a related positive feedback; the solar radiation absorbed by the surface-atmosphere system increases because the diminished cloud amount causes a reduction of reflected solar radiation by the atmosphere. The situation is further complicated by climate-induced changes in both cloud vertical structure and cloud optical properties, which result in additional infrared and solar feedbacks [*Cess and Potter*, 1988].

In this intercomparison, cloud effects were isolated by separately averaging a model's clear-sky TOA fluxes [*Charlock and Ramanathan*, 1985; *Ramanathan*, 1987; *Cess and Potter*, 1988], such that in addition to evaluating climate sensitivity for the globe as a whole, it was also possible to consider an equivalent "clear-sky" Earth. In other words, a model's clear-sky TOA infrared and solar fluxes were separately stored during integration and then globally averaged by use of appropriate area weighting. When used in conjunction with (3), a single model integration thus provided not only the global climate sensitivity parameter but also a second sensitivity parameter that refers to a clear-sky Earth with the same climate as that with clouds present. In effect, GCM output was processed in a manner similar to the way in which data is processed in the Earth Radiation Budget Experiment [*Ramanathan et al.*, 1989], an experiment that also produces an equivalent clear-sky Earth.

The choice of a model intercomparison simulation was governed by several factors. Ideally, the climate simulation should refer to a relevant situation, such as increasing the atmospheric CO_2 concentration. Only five of the 19 models, however, have so far been employed for that purpose. Furthermore, these models have, at least in part, differing climate sensitivities because their control (that is, present-day) climates are different [*Spelman and Manabe*, 1984; *Cess and Potter*, 1988]. If a model produces a control climate

TABLE 1. Summary of the GCMs Used in the Present Intercomparison

Model	Investigator(s)
Bureau of Meteorology Research Centre, Melbourne (BMRC)	B. J. McAvaney and L. Rikus
Canadian Climate Centre (CCC)	G. J. Boer and J.-P. Blanchet
Colorado State University (CSU)	D. A. Randall
Department of Numerical Mathematics of the U.S.S.R. Academy of Sciences (DNM)	V. Dymnikov and V. Galin
Direction de la Météorologie National, Toulouse (DMN)	J. F. Royer and M. Déqué
European Centre for Medium-Range Weather Forecasts (ECMWF)	J.-J. Morcrette
European Centre for Medium-Range Weather Forecasts/University of Hamburg (ECHAM)	E. Roeckner and U. Schlese
Geophysical Fluid Dynamics Laboratory (GFDL I and II)	R. T. Wetherald
Laboratoire de Météorologie Dynamique, Paris (LMD)	H. Le Treut and X.-Z. Li
Main Geophysical Observatory, Leningrad (MGO)	V. P. Meleshko, A. P. Sokolov, and D. A. Sheinin
Meteorological Research Institute, Japan (MRI)	I. Yagai
NASA Goddard Institute for Space Studies (GISS)	A. Lacis and A. D. Del Genio
NCAR Community Climate Model, Version 0 (CCM0)	W. M. Washington
NCAR Community Climate Model, Version 1 (CCM1)	A. Slingo and J. T. Kiehl
NCAR Community Climate Model/Lawrence Livermore National Laboratory (CCM/LLNL)	S. J. Ghan and K. E. Taylor
Oregon State University/Institute for Atmospheric Physics, Beijing (OSU/IAP)	X.-Z. Liang and X.-H. Zhang
Oregon State University/Lawrence Livermore National Laboratory (OSU/LLNL)	R. D. Cess, G. L. Potter and W. L. Gates
United Kingdom Meteorological Office (UKMO)	J. F. B. Mitchell

There are two GFDL models.

that is either too warm or too cold, then it will respectively produce a climate sensitivity parameter that is too small or too large, and clearly, the intercomparison simulation had to be designed to eliminate this effect. There was also a practical constraint: the CO_2 simulations require large amounts of computer time for equilibration of the rather primitive ocean models that have been used in these numerical experiments.

An attractive alternative that eliminated both of the above mentioned difficulties was to adopt ±2°K sea surface temperature (SST) perturbations, in conjunction with a perpetual July simulation, as a surrogate climate change for the sole purpose of intercomparing model climate sensitivity [*Cess and Potter*, 1988]. This procedure is in essence an inverse climate change simulation. Rather than introducing a forcing G into the models and then letting the climate respond to this forcing, the climate change is instead prescribed, and the models in turn produce their respective forcings in accordance with (1). This procedure eliminated the substantial computer time required for equilibration of the ocean. The second advantage was that because the same SSTs are prescribed [*Alexander and Mobley*, 1976], all of the models have very similar control surface temperatures because land temperatures are tightly coupled, through atmospheric transport, to the SSTs. The models then all produced a global-mean ΔT_s, for the −2° to +2°K SST change, that was close to 4°K, and different model sensitivities in turn resulted in different values for G.

The perpetual July simulation eliminated another problem. The present study focuses solely on atmospheric feedback mechanisms, and, with one exception, inspection of output from the models showed that climate feedback caused by changes in snow and ice cover was suppressed through use of a fixed sea ice constraint and because the perpetual July simulations produced very little snow cover in the northern hemisphere. For this reason we adopted global averages rather than the 60°S to 60°N averages as used in an earlier study [*Cess and Potter*, 1988].

3. General Circulation Model Descriptions

The 19 atmospheric GCMs employed in the present investigation are listed in Table 1, and for future reference these will be designated by the acronyms given in parentheses. The respective documentation references are given in Table 2. Several of the models contain modifications that were made after the documentation reference was written, and in these cases the modification is referenced either to a subsequent publication or to an appendix of the present paper. Brief descriptions of the 19 GCMs are given in Table 3, while Tables 4 and 5 respectively summarize their convective and stratiform cloud parameterizations.

Several of the GCMs have common origins. For example, the sole difference between the Geophysical Fluid Dynamics Laboratory (GFDL) I and II models is that GFDL I employs prescribed cloud albedos, whereas GFDL II includes a parameterization for cloud albedo as a function of cloud water content, in addition to including a dependence of cloud emissivity upon water content solely for ice clouds. The NCAR (National Center for Atmospheric Research) Community Climate Model (CCM) version 0 (CCM0) and version 1 models refer to the standard versions 0 and 1 of the NCAR CCM, while CCM/Lawrence Livermore National Laboratory (LLNL) is CCM1 with a revised solar radiation code and the incorporation of cloud albedos as a function of cloud water content. The Oregon State University/Institute for Atmospheric Physics (OSU/IAP) and OSU/LLNL GCMs are two-level models that contain modifications to the standard Oregon State University GCM. For the OSU/IAP model these consist of revisions to both the numerical technique and the convective adjustment parameterization, while the OSU/LLNL GCM contains a revised solar radiation code. As a consequence of the correction of a coding error, results presented here for the OSU/IAP GCM differ from those presented earlier [*Cess et al.*, 1989]. The Euro-

TABLE 2. Summary of Documentation References for the 19 GCMs

Model	Reference
BMRC	*Hart et al.* [1990]
CCC	*Boer et al.* [1984], see Appendix A for modifications.
CSU	*Arakawa and Lamb* [1977], *Suarez et al.* [1983], *Randall et al.* [1989]
DNM	*Marchuk et al.* [1986]
DMN	*Coiffier et al.* [1987], *Cariolle et al.* [1990]
ECHAM	Same as ECMWF. See *Morcrette* [1990] for radiation modifications.
ECMWF	ECMWF forecast model. Adiabatic part (Research Manual 2), physical parameterizations (Research Manual 3). *Meteorological Bulletin*, 2nd ed., 1988. ECMWF, Reading, United Kingdom. See *Slingo* [1987] for a description of the cloud parameterization and *Morcrette* [1990] for radiation modifications.
GFDL I	*Wetherald and Manabe* [1988].
GFDL II	See Appendix B for a description of the cloud optical property modifications.
LMD	*Sadourny and Laval* [1984]. See *Le Treut and Li* [1988] for cloud modifications.
MGO	*Sokolov* [1986]
MRI	*Tokioka et al.* [1984].
GISS	*Hansen et al.* [1983].
CCM0	*Washington and Meehl* [1984].
CCM1	*Williamson et al.* [1987].
CCM/LLNL	*Williamson et al.* [1987]. See Appendix C for solar radiation and cloud optical property modifications.
OSU/IAP	*Zeng et al.* [1989], see Appendix D for modifications.
OSU/LLNL	*Ghan et al.* [1982], see *Cess et al.* [1985] for solar radiation modification.
UKMO	*Slingo* [1985], see *Wilson and Mitchell* [1987] for modifications.

pean Centre for Medium-Range Weather Forecasts/ University of Hamburg (ECHAM) GCM, relative to ECMWF, has a revised radiation code and a coarser (factor of 2) horizontal resolution.

As described in Tables 4 and 5, all of the models treat two cloud types: stratiform (large scale) and convective clouds. Except in the Bureau of Meteorology Research Centre (BMRC), European Centre for Medium-Range Weather Forecasts (ECMWF), ECHAM, and Main Geophysical Observatory (MGO) models, stratiform clouds are formed in an atmospheric layer when the relative humidity exceeds a prescribed threshold value, which varies among models from 90 to 100%. The models then either prescribe the cloud cover in their respective horizontal grid areas, which vary in size from 2.8° by 2.8° to 5° by 7.5° in latitude by longitude or calculate it as a function of relative humidity. In the ECMWF, ECHAM, and MGO GCMs, vertical velocity and lapse rate are also used as cloud predictors.

The procedure for convective clouds is far less consistent. The CCC, the two GFDL, and the three CCM GCMs generate convective clouds according to the presence of convective adjustment. However, the fraction of the grid area that is covered by convective cloud varies from 30 to 100% among these models. In the remaining models a parameterization is used that relates the convective cloud fraction to the convective precipitation rate.

4. CLOUD COVER RESPONSES

Global cloud amounts, and changes in this quantity for the ±2°K SST perturbations, are summarized in Table 6 for the 19 models. (These models are listed in the order of their respective climate sensitivities as given in the following section.) Here the cloud amounts refer to the cold simulation

TABLE 3. Brief Descriptions of the GCMs

Model	Number Levels	Solution Technique, Spectral Truncation	Horizontal Resolution, longitude times latitude	Convection Parameterization	Diurnal Cycle	Soil Moisture
BMRC	9	spectral (R21)	5.6°×3.2°	penetrating convection*	no	computed
CCC	10	spectral (T21)	5.6°×5.6°	moist adiabatic	yes	computed
CSU	9	finite difference	5°×4°	penetrating convection†	yes	prescribed
DNM	7	finite difference	5°×4°	moist adiabatic	no	computed
DMN	20	spectral (T42)	2.8°×2.8°	penetrating convection†	yes	computed
ECHAM	16	spectral (T21)	5.6°×5.6°	penetrating convection*	no	computed
ECMWF	19	spectral (T42)	2.8°×2.8°	penetrating convection*	yes	computed
GFDL	9	spectral (R15)	7.5°×4.5°	moist adiabatic	no	computed
LMD	11	finite difference	5.6°×3.6°	penetrating convection*	no	computed
MGO	9	spectral (T21)	5.6°×5.6°	penetrating convection*	no	computed
MRI	12	finite difference	5°×4°	penetrating convection†	yes	computed
GISS	9	finite difference	10°×7.8°	penetrating convection†	yes	computed
CCM0	9	spectral (R15)	7.5°×4.5°	moist adiabatic	no	computed
CCM1	12	spectral (R15)	7.5°×4.5°	moist adiabatic	no	prescribed
CCM/LLNL	12	spectral (R15)	7.5°×4.5°	moist adiabatic	no	prescribed
OSU/IAP	2‡	finite difference	5°×4°	penetrating convection†	yes	computed
OSU/LLNL	2‡	finite difference	5°×4°	penetrating convection†	yes	computed
UKMO	11	finite difference	7.5°×5°	penetrating convection†	yes	prescribed

The horizontal resolution of the spectral models is that of the Gaussian grid.
*Kuo parameterization.
†Mass-flux parameterization.
‡Four levels are used for radiation and cloud formation calculations.

TABLE 4. Summary of Convective Cloud Parameterizations

Model	Cloud Generation and Fraction	Optical Properties	Comments
BMRC	cloud fraction function of relative humidity	prescribed	convective and stratiform clouds not distinguished
CCC	same as BMRC	function of cloud water content	no clouds in bottom layer nor above 100 mbar
CSU	no clouds in radiation sense unless convection penetrates above 400 mbar, then 100% cloudiness from 400 mbar to highest level reached by convection	prescribed (optically thick)	
DNM	same as BMRC	prescribed	no clouds below 930 mbar nor above 290 mbar
DMN	cloud fraction function of convective precipitation	function of cloud water content	no clouds above 65 mbar
ECMWF and ECHAM	convective precipitation used as cloud fraction predictor with upper limit of 80% cloudiness	function of cloud water content	no clouds in top and bottom layers
GFDL I	no clouds unless saturation occurs (relative humidity = 99%), then 100% cloudiness	prescribed	convective and stratiform clouds not distinguished
GFDL II	same as GFDL I	albedos functions of cloud water content, emissivities prescribed except for ice clouds	Same as GFDL I
LMD	same as OSU/IAP	function of cloud water content	
MGO	same as ECMWF	prescribed	no clouds in bottom layer nor above 150 mbar
MRI	same as CSU	prescribed (optically thick)	
GISS	cloud fraction proportional to pressure thickness of all layers up to cloud top	prescribed: optical depth = 8 per 100 mbar thickness	no clouds above 100 mbar
CCM0 and CCM1	no clouds unless convective adjustment necessary, then 30% cloudiness	prescribed	no clouds in bottom layer
CCM/LLNL	same as CCM1	visible optical depths and emissivities functions of cloud water content	no clouds in bottom layer
OSU/IAP	penetrative convection parameterization, 0% or 100% cloudiness	albedos and emissivities step functions of temperature at T = −40°	convective cloud formation only in 200–400 mbar layer or at 800 mbar
OSU/LLNL	same as OSU/IAP	visible optical depths and emissivities step functions of temperature at T = −40°C	convective cloud formation only in 200–400 mbar and 800–1000 mbar layers
UKMO	cloud fraction proportional to maximum parcel size in moist convection	prescribed	no clouds in top layer

($\Delta SST = -2°K$), which constitutes the "control run" for our present SST warming simulations. Although there is a substantial variation in cloud amount among the models, this is in part due to the fact that the two models producing the largest cloud amounts (Canadian Climate Center (CCC) and Colorado State University (CSU)) contain significant cirrus having extremely small optical depths. Note that all of the models are consistent as to the sign of the change in cloud amount (i.e., cloud cover decreases for climate warming), although the magnitude of this change varies significantly from model to model.

The change in cloud cover, however, provides only limited information with regard to interpreting cloud feedback. This, unfortunately, is also the case with respect to changes in cloud vertical distribution. The reason is that many of the models incorporate cloud albedos and emissivities that are dependent upon cloud water content, such that changes in these optical properties occur in conjunction with changes in cloud horizontal and vertical distributions. For this reason the issue of changes in cloud horizontal and vertical distributions will not be addressed in this study.

5. FEEDBACK INTERCOMPARISON AND INTERPRETATION

Before discussing feedback processes, the TOA fluxes that generate these quantities are first considered. In addition to global (entire Earth) fluxes, separate global-mean clear and overcast fluxes are also evaluated from the model outputs. Global averaging for all the TOA fluxes (global, clear, and overcast) is performed by employing conventional area weighting in contrast, for example, to clear-sky area

TABLE 5. Summary of Stratiform (Supersaturation) Cloud Parameterizations

Model	Cloud Generation and Fraction	Optical Properties	Comments
BMRC	cloud fraction function of relative humidity and lapse rate	prescribed	no clouds in bottom layer nor above 200 mbar
CCC	cloud fraction function of relative humidity	function of cloud water content	no clouds in bottom layer nor above 100 mbar
DNM	same as BMRC	prescribed	no clouds above 930 mbar nor above 290 mbar
CSU	no clouds unless saturation occurs (RH = 100%), then 100% cloudiness	visible optical depths and emissivities dependent on temperature	clouds in bottom layer can be arbitrarily thin
DMN	cloud fraction function of relative humidity	function of cloud water content	no clouds above 65 mbar
ECMWF and ECHAM	cloud fraction predictors are RH, vertical velocity and lapse rate	function of cloud water content	no clouds in top and bottom layers
GFDL I	no clouds unless saturation occurs (RH = 99%), then 100% cloudiness	prescribed	convective and stratiform clouds not distinguished
GFDL II	same as GFDL I	albedos dependent on cloud water content, emissivities prescribed except for ice clouds	same as for GFDL I
LMD	cloud fraction function of partial condensation	function of cloud water content	
MGO	same as ECMWF, but different parameters	prescribed	no clouds in bottom layer nor above 150 mbar
MRI	same as CSU	prescribed	no clouds in planetary boundary layer
GISS	no clouds unless saturation occurs (RH = 100%), then cloud fraction equals saturated grid fraction	visible optical depths prescribed function of pressure; emissivities calculated from visible optical depths	no clouds above 100 mbar
CCM0 and CCM 1	no clouds unless saturation occurs (RH = 99%), then 100% cloudiness (100% and 95% for CCM1)	prescribed	no clouds in bottom layer
CCM/LLNL	no clouds unless saturation occurs (RH = 100%), then 100% cloudiness	visible optical depths and emissivities dependent on cloud water content	no clouds in bottom layer
OSU/IAP	no clouds unless saturation occurs (RH = 100% for 400–800 mbar, RH = 90% for 600–80 mbar), then 100% cloudiness	albedos and emissivities step functions of temperature at T = −40°C	stratiform cloud formation only in 400–800 mbar layer
OSU/LLNL	same as OSU/IAP	visible optical depths and emissivities step functions of temperature at T = −40°C	same as OSU/IAP
UKMO	cloud fraction function of relative humidity	prescribed	no clouds in top layer

weighting of clear fluxes. The clear and overcast fluxes are thus arithmetically averaged over longitude to produce zonal means, and denoting these by $Y(\phi)$, with ϕ = latitude, then the global average, $\bar{Y}$ is obtained from

$$\bar{Y} = \int_{-\pi/2}^{\pi/2} Y(\phi) \cos \phi \, d\phi \tag{6}$$

In the terminology of *Cess and Potter* [1987] the clear flux evaluation refers to Method I.

Tables 7 and 8 summarize, respectively, the emitted infrared and net downward solar TOA fluxes for the ΔSST = −2 K "control" simulation. In addition to global fluxes, the separate globally averaged clear and overcast fluxes are also summarized. The agreement of the clear TOA infrared fluxes, shown in Table 7, is less than what might have been anticipated. Bear in mind that this is more than just an intercomparison of the models' infrared radiation codes, since the TOA infrared flux additionally depends upon both lapse rate and water vapor abundance.

As would be expected, there is less agreement for the overcast fluxes since they involve intermodel differences in cloud infrared optical properties, cloud-top temperatures, and the uncertain partitioning into clear and overcast fractions in the case of "thin" clouds. The agreement in global fluxes is better, despite the fact that this composite of clear and overcast fluxes contains the additional uncertainty associated with cloud amount (Table 6). This is probably a consequence of model tuning. The situation is much the same with respect to the net downward solar flux summa-

TABLE 6. Percentage Cloud Amount, A_c, for the ΔSST = −2°K Simulations and ΔA_c for the ΔSST = ±2°K Change (+2°K Simulation Minus −2°K Simulation)

Model	A_c, %	ΔA_c, %
CCC	62	−4.3
ECMWF	50	−1.1
MGO	52	−0.2
DNM	48	−2.0
GFDL II	56	−1.1
DMN	40	−0.9
CSU	72	−4.4
OSU/IAP	60	−2.5
OSU/LLNL	58	−1.3
BMRC	48	−2.8
MRI	40	−1.4
GFDL I	49	−0.3
UKMO	52	−2.1
CCM1	48	−0.7
CCM/LLNL	58	−2.8
LMD	58	−2.5
ECHAM	57	−3.5
CCM0	53	−4.4
GISS	52	−1.3
Mean	53	−2.1
Standard Deviation	8	1.3

TABLE 8. Net Downward Solar Fluxes at the Top of the Atmosphere for the ΔSST = −2°K Simulations

Model	Flux, W m^{-2}		
	Clear	Overcast	Global
CCC	291	229	250
ECMWF	300	219	258
MGO	303	190	245
DNM	264	192	228
GFDL II	280	195	235
DMN	286	136	242
CSU	288	210	231
OSU/IAP	273	149	203
OSU/LLNL	284	162	220
BMRC	294	187	245
MRI	285	191	242
GFDL I	281	167	228
UKMO	294	147	233
CCM1	278	187	233
CCM/LLNL	277	183	224
LMD	298	220	253
ECHAM	275	162	215
CCM0	271	178	227
GISS	281	190	233
Mean	284	184	234
Standard Deviation	10	26	14

rized in Table 8. That the clear solar flux shows slightly greater disagreement than does the infrared is probably a consequence of intermodel differences in surface albedo.

The climate sensitivity parameter as defined by (3) is evaluated for the globe as a whole and also for "clear" and "overcast" conditions; i.e., sensitivity parameters employing respectively clear and overcast fluxes. These results are summarized in Table 9 and in Figure 1. While the models exhibit notable agreement in the clear sensitivity parameter, there is, as might be anticipated, considerable variation in the overcast quantity. An important point, to which we will return, is that the nearly threefold variation in the global sensitivity parameter is largely attributable to cloud feedback processes, since there is a much smaller variation in clear-sky sensitivity. This point is clearly demonstrated by the graphical summary of the clear-sky and global sensitivity parameters shown in Figure 1, where the ordering of the models is the same as in Table 9.

As previously discussed, the perpetual July simulation suppressed the feedback due to variable snow and ice coverage, so that the primary clear-sky feedback is water-vapor feedback. On average the 19 GCMs produced a clear-sky sensitivity parameter of 0.47 K m^2 W^{-1}, as is consistent with the prior discussion of positive water-vapor feedback concerning (5) versus (4). One exception is the ECMWF GCM, for which there is modest positive snow-

TABLE 7. Emitted Infrared Fluxes at the Top of the Atmosphere for the ΔSST = −2°K Simulations

Model	Flux, W m^{-2}		
	Clear	Overcast	Global
CCC	270	248	255
ECMWF	273	194	240
MGO	271	201	235
DNM	259	221	242
GFDL II	269	221	243
DMN	260	212	247
CSU	259	209	222
OSU/IAP	277	198	230
OSU/LLNL	271	193	228
BMRC	280	213	249
MRI	258	199	236
GFDL I	269	194	234
UKMO	267	195	235
CCM1	275	218	243
CCM/LLNL	277	222	245
LMD	268	238	250
ECHAM	250	205	234
CCM0	271	180	224
GISS	253	215	234
Mean	267	209	238
Standard Deviation	8	17	9

TABLE 9. Climate Sensitivity Parameter

Model	λ, K m^2 W^{-1}		
	Clear	Overcast	Global
CCC	0.42	0.24	0.39
ECMWF	0.57	0.29	0.40
MGO	0.54	0.37	0.44
DNM	0.44	0.49	0.45
GFDL II	0.46	0.40	0.45
DMN	0.44	0.57	0.50
CSU	0.46	0.45	0.50
OSU/IAP	0.40	0.45	0.52
OSU/LLNL	0.48	0.53	0.52
BMRC	0.52	0.33	0.54
MRI	0.47	1.20	0.60
GFDL I	0.48	0.70	0.60
UKMO	0.53	0.54	0.61
CCM1	0.43	3.67	0.70
CCM/LLNL	0.49	0.72	0.76
LMD	0.43	1.42	0.89
ECHAM	0.47	0.60	1.11
CCM0	0.45	−2.58	1.11
GISS	0.52	−3.71	1.23
Mean	0.47		0.65
Standard Deviation	0.05		0.26

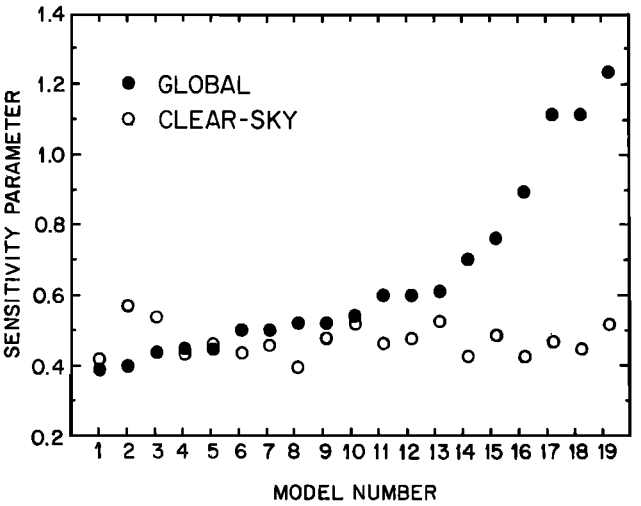

Fig. 1. Clear-sky and global sensitivity parameters (K m^2 W^{-1}) for the 19 GCMs. The model numbers correspond to the ordering in Table 9.

albedo feedback that partially explains why this model has the largest clear-sky sensitivity parameter. Furthermore, as will shortly be discussed, there is a subtle solar feedback mechanism that contributes to some of the modest variation in clear-sky sensitivity among the models.

To better understand this intercomparison of sensitivity parameters, consider the separate infrared and solar feedback derivatives, $\Delta F/\Delta T_s$ and $\Delta Q/\Delta T_s$, that appear within (3). These are summarized in Tables 10 and 11. To illustrate how these individual infrared and solar feedback processes may be interpreted, it will suffice to consider three separate pairs of GCMs. The CSU and OSU/LLNL GCMs comprise one pair since they have nearly identical global sensitivity parameters (Table 9). But as will be shortly emphasized, this is the result of several compensating effects. The GFDL I and II models are the second pair since here there is a means

TABLE 10. Infrared Feedback Derivatives $\Delta F/\Delta T_s$

Model	$\Delta F/\Delta T_s$, W m^{-2} K^{-1}		
	Clear	Overcast	Global
CCC	2.53	1.22	2.50
ECMWF	2.46	0.62	1.65
MGO	2.18	2.74	2.53
DNM	2.45	2.85	2.92
GFDL II	2.22	2.13	2.28
DMN	2.37	2.50	2.56
CSU	2.22	2.42	2.98
OSU/IAP	2.67	1.10	2.30
OSU/LLNL	2.46	1.20	2.20
BMRC	2.04	3.54	3.13
MRI	2.35	1.50	2.19
GFDL I	2.17	1.91	2.10
UKMO	2.10	2.83	2.98
CCM1	2.47	1.34	2.30
CCM/LLNL	2.35	1.27	2.15
LMD	2.44	1.62	2.17
ECHAM	2.60	2.16	2.80
CCM0	2.41	1.29	3.00
GISS	1.93	1.92	2.04
Mean	2.34	1.90	2.46
Standard Deviation	0.20	0.76	0.41

TABLE 11. Solar Feedback Derivatives $\Delta Q/\Delta T_s$

Model	$\Delta Q/\Delta T_s$, W m^{-2} K^{-1}		
	Clear	Overcast	Global
CCC	0.12	−2.92	−0.10
ECMWF	0.74	−2.82	−0.83
MGO	0.32	0.05	0.25
DNM	0.17	0.81	0.70
GFDL II	0.06	−0.38	0.07
DMN	0.11	0.75	0.55
CSU	0.03	0.19	0.99
OSU/IAP	0.18	−1.10	0.36
OSU/LLNL	0.39	−0.69	0.30
BMRC	0.13	0.50	1.26
MRI	0.20	0.67	0.53
GFDL I	0.07	0.48	0.44
UKMO	0.11	0.99	1.27
CCM1	0.16	1.06	0.87
CCM/LLNL	0.29	−0.12	0.84
LMD	0.14	0.91	1.04
ECHAM	0.47	0.51	1.90
CCM0	0.14	1.60	2.08
GISS	0.00	2.19	1.22
Mean	0.20	0.14	0.72
Standard Deviation	0.18	1.30	0.69

of directly appraising a feedback due to cloud optical properties. Recall that GFDL I adopts prescribed cloud albedos, whereas in GFDL II the cloud albedos are dependent upon cloud liquid water content and thus increase, on average, as the climate warms, resulting in a negative climate feedback mechanism [e.g., *Petukhov et al.*, 1975; *Somerville and Remer*, 1984]. A similar difference exists between the CCM1 and CCM/LLNL models, which constitute the third pair.

Note from Table 10 that the most significant difference between the CSU and OSU/LLNL models concerns the overcast $\Delta F/\Delta T_s$, and this may be attributed to differences in the models' changes in vertical cloud distribution. For the OSU/LLNL model, climate warming produces an increase in high clouds over the northern hemisphere (NH) tropics and mid-latitudes that are primarily optically thick convective clouds [*Cess and Potter*, 1988]. Thus, in terms of global-mean overcast conditions, global warming produces a relative increase in optically thick high, and hence cold, clouds that emit less radiation than do low clouds. The net effect is that the overcast $\Delta F/\Delta T_s$ is roughly half the value for clear regions (Table 10). Thus, relative to a clear-sky planet, and with reference to (3), this by itself constitutes a positive feedback mechanism since it increases the climate sensitivity parameter. In physical terms the climate-induced change in cloud vertical structure means that as the surface-atmosphere warms its ability to emit heat is diminished; i.e., a positive climate feedback.

But this positive feedback is partially mitigated by an associated negative feedback due to the warming-induced decrease in cloud amount (Table 6). If there were no reduction in cloud amount, then combination of the clear and overcast $\Delta F/\Delta T_s$ values of Table 10, utilizing the 58% cloud cover of Table 6, yields a global $\Delta F/\Delta T_s$ value of 1.9 W m^{-2}, in contrast to the actual 2.2 W m^{-2} result. The point is that the reduction in cloud amount enhances the Earth's ability to emit heat to space, and this negative feedback partially compensates the positive feedback associated with cloud vertical redistribution.

The situation is quite different for the CSU model, since the overcast $\Delta F/\Delta T_s$ value in this case is slightly greater than the clear value. This model also exhibits a general increase in high clouds, but this increase is concentrated at mid-latitudes and refers primarily to optically thin cirrus, in contrast to thick convective clouds for the OSU/LLNL model. Moreover, to mimic a dependence upon cloud liquid water content, the emissivity of the CSU model's cirrus clouds is dependent upon cloud temperature, so that a vertical redistribution of cirrus to higher altitudes reduces the cloud emissivity. While this amplifies the reduction in the cloud's infrared emission, it likewise increases its transmissivity, allowing an increase in the upwelling radiation from below that passes through the cloud. This phenomenon, coupled with an actual reduction in high convective clouds over the tropics, plausibly explains the clear versus overcast $\Delta F/\Delta T_s$ values of Table 10. Then, as in the OSU/LLNL model, the warming-induced reduction in cloud amount produces a negative feedback that here results in a global $\Delta F/\Delta T_s$ value that exceeds its component clear and overcast values.

To summarize this discussion, relative to clear regions there is a substantial positive overcast infrared feedback in the OSU/LLNL GCM due to cloud vertical redistribution, but this is partially compensated by a negative feedback due to the change in cloud amount. For the CSU GCM, on the other hand, these separate effects are both modest negative feedbacks.

Comparable logic applies to the solar feedbacks (Table 11). For the OSU/LLNL GCM the negative overcast $\Delta Q/\Delta T_s$ value denotes a negative feedback that is caused by the large albedo of the enhanced high convective clouds. For climate warming this causes the planetary albedo to increase, thus decreasing absorbed solar radiation. Conversely, the decrease in cloud amount is now a positive feedback (since the Earth-atmosphere system absorbs more solar radiation) that largely offsets the negative feedback due to cloud vertical redistribution, resulting in little difference between the global and clear $\Delta Q/\Delta T_s$ values. For the CSU model, on the other hand, both are positive feedbacks, with cloud vertical redistribution causing a slight reduction in planetary albedo.

Next, note that the differences in the global $\Delta F/\Delta T_s$ values for the two models (Table 10) are nearly offset by similar differences in their $\Delta Q/\Delta T_s$ values (Table 11). Thus while the two models produce comparable climate sensitivity parameters (Table 9), their individual components of cloud feedback are quite different but essentially compensatory. Within both models the net effect of clouds, relative to a clear-sky Earth, is to enhance climate sensitivity by a mere 8%.

Turning next to the GFDL I and II models, recall that GFDL II contains a negative feedback due to the dependence of cloud albedo upon cloud liquid water content, and the sensitivity parameters of Table 9 are consistent with this expectation. This is further consistent with their overcast $\Delta Q/\Delta T_s$ values (Table 11), with II and I producing, respectively, negative and positive overcast solar feedbacks.

A similarly straightforward argument does not, however, apply to the CCM1 versus CCM/LLNL models, for which the primary difference is that the latter incorporates cloud albedos as a function of cloud water content (Tables 4 and 5). Like the GFDL II versus I comparison, the overcast $\Delta Q/\Delta T_s$ results of Table 11 clearly indicate that CCM/LLNL contains, relative to CCM1, a negative solar overcast feedback and, as with the GFDL comparison, this is consistent with cloud albedos being dependent upon cloud liquid water content. But unlike the GFDL comparison this does not translate into a negative solar global feedback since the global $\Delta Q/\Delta T_s$ values for CCM/LLNL and CCM1 are quite similar.

What appears to be happening is that the negative solar overcast feedback in CCM/LLNL is being compensated by a positive cloud-amount feedback, since from Table 6 CCM/LLNL produces a greater decrease in cloud amount than does CCM1 (recall that this by itself is a positive solar feedback process). Furthermore, this enhanced cloud reduction refers primarily to low clouds, which have little impact upon infrared emission, and this is consistent with the fact that for the two models the $\Delta F/\Delta T_s$ results of Table 10 do not indicate a CCM/LLNL cloud-amount infrared feedback.

The interesting point is that two separate pairs of GCMs, GFDL II versus I and CCM/LLNL versus CCM1, produce both similar and differing results concerning climate feedback as induced by the dependence of cloud albedos upon cloud water content. The similarity is that both pairs indicate that this produces a negative overcast feedback. The difference is that the CCM pair suggests an additional compensatory positive cloud-amount feedback that does not occur in the GFDL pair.

As previously discussed, $\Delta Q/\Delta T_s = 0$ in the absence of interactive feedbacks. Although of small magnitude the clear-sky $\Delta Q/\Delta T_s$ values in Table 11 show considerable variability. Typically, one expects $\Delta Q/\Delta T_s$ for clear skies to be a small positive quantity due again to positive water-vapor feedback, since the water-vapor increase associated with a warmer atmosphere produces more solar absorption by the atmosphere. A typical value, determined using the solar radiation model of *Cess and Vulis* [1989], and adopting the *McClatchey et al.* [1971] mid-latitude summer versus winter atmospheres, is

$$\Delta Q/\Delta T_s = 0.2 \text{ W m}^{-2} \text{ °C}^{-1} \quad (7)$$

The departures from this value in Table 11 are greater than anticipated and do not appear to reflect differences in the GCMs' solar radiation codes and hydrological cycles. Rather, they seem to be due to differences in the respective models' cloud responses. For example, over ocean areas the clear-sky $\Delta Q/\Delta T_s$ value of the CSU GCM is that of (7). But for land it is $\Delta Q/\Delta T_s = -0.5 \text{ W m}^{-2} \text{ K}^{-1}$, and this negative value seems to be due to a climate-induced change in clear-sky regions relative to the underlying surface; i.e., the model's cloud response is such that clear-sky areas are shifted to regions of higher surface albedo.

For the CCM/LLNL model, on the other hand, the value of $\Delta Q/\Delta T_s$ is somewhat larger than that given by (7). Here the explanation is that as the climate warms there is a shift in clear regions from oceans to continents, effectively reducing the clear-sky surface albedo and thus increasing $\Delta Q/\Delta T_s$. When this effect is suppressed within the CCM/LLNL model, it is found that $\Delta Q/\Delta T_s$ is reduced from 0.29 W m^{-2} K^{-1} (Table 11) to 0.17 W m^{-2} K^{-1}.

6. CLOUD-RADIATIVE FORCING AND CLOUD FEEDBACK

It will be useful, both scientifically and tutorially, to rephrase the GCM results of the previous section in terms of cloud radiative forcing and cloud feedback. But before doing so, it will be helpful to emphasize that there presently exist differing definitions of cloud feedback. For example, *Wetherald and Manabe* [1988] have addressed cloud feedback by performing two simulations, one with computed clouds and the other holding clouds fixed at their control climate values. Thus in this definition cloud feedback is referenced to the simulation in which clouds are invariant to the change in climate, while all other feedback processes are operative. For their CO_2 doubling simulations, *Wetherald and Manabe* [1988] found that cloud feedback amplified global warming by the factor 1.3.

Hansen et al. [1984], again for a CO_2 doubling, employed a radiative-convective model to diagnose three categories of feedback mechanisms within the Goddard Institute for Space Studies (GISS) GCM: water-vapor, snow/ice-albedo and cloud feedbacks. As did *Wetherald and Manabe* [1988], Hansen et al., found that cloud feedback produced a 1.3 factor amplification. However, their feedback definition differs from that of Wetherald and Manabe; it is referenced not only to fixed clouds but also to the absence of both water-vapor feedback and snow/ice-albedo feedback. When their results are reformulated in terms of Wetherald and Manabe's definition, their cloud feedback amplification factor is 1.8.

The present study adopts yet a third definition of cloud feedback, but one that has the advantage of being related to a measurable quantity, namely, cloud radiative forcing [*Charlock and Ramanathan*, 1985; *Ramanathan*, 1987; *Ramanathan et al.*, 1989]. Simply stated, cloud radiative forcing refers to the radiative impact of clouds upon the Earth's radiation budget as determined at the TOA. Letting $H = Q - F$ represent the net heating of the surface-atmosphere system, while $H_c = Q_c - F_c$ is the cloud-free or clear-sky value, then cloud radiative forcing is defined as

$$\text{CRF} = H - H_c = (F_c - F) - (Q_c - Q) \tag{8}$$

Positive values of CRF thus indicate that clouds warm the system while negative values correspond to cooling. Since $F_c - F$ is generally positive, this reflects the greenhouse warming caused by clouds; the opposite effect due to reflection of solar radiation will cool the system.

Combination of (1), (2), (3), and (8) yields

$$\lambda/\lambda_c = 1 + \Delta\text{CRF}/G \tag{9}$$

where ΔCRF is the change in cloud radiative forcing as induced by the change in climate, and λ_c is the clear-sky climate sensitivity parameter. Note that ΔCRF includes embedded changes in cloud amount, vertical distribution, and optical properties; it is this quantity that represents cloud feedback. A positive ΔCRF resulting from climate warming means that cloud feedback acts to amplify the warming and is thus a positive feedback, while the opposite is true for a negative ΔCRF.

Conceptually, cloud feedback should be related to a change in cloud radiative forcing, and (9) clearly illustrates this expectation. Note that in the absence of cloud feedback (i.e., $\Delta\text{CRF} = 0$), the global sensitivity parameter equals that for clear skies. In turn, a departure of λ/λ_c from unity is a measure of cloud feedback, with $\lambda/\lambda_c > 1$ denoting a positive feedback. An important point is that cloud forcing, for the Earth's present climate, is a measurable quantity; the Earth Radiation Budget Experiment (ERBE) is currently providing this information [*Ramanathan et al.*, 1989].

TABLE 12. Solar, Infrared, and Net Cloud Forcing for the ΔSST = −2°K Simulations

Model	CRF, W m^{-2}		
	Solar	Infrared	Net
CCC	−41	15	−26
ECMWF	−41	33	−8
MGO	−58	36	−22
DNM	−35	17	−19
GFDL II	−46	26	−20
DMN	−44	13	−30
CSU	−58	37	−21
OSU/IAP	−70	48	−23
OSU/LLNL	−63	44	−19
BMRC	−49	31	−18
MRI	−33	22	−11
GFDL I	−53	36	−17
UKMO	−61	31	−30
CCM1	−45	32	−13
CCM/LLNL	−54	32	−22
LMD	−45	18	−27
ECHAM	−60	15	−45
CCM0	−49	47	−2
GISS	−48	19	−30
Mean	−50	29	−21
Standard Deviation	10	11	9

This definition of cloud feedback differs from the previously discussed definitions that refer to the use of fixed clouds; here the reference state is a clear-sky Earth. Fixed clouds can, in fact, give rise to a change in CRF and produce cloud feedback as here defined. For example, overcast regions emit less TOA infrared radiation than do clear regions, so that for global warming there should be a greater increase in clear emission relative to overcast emission; i.e., an increase in infrared CRF.

The conventional interpretation of climate feedback is that it modifies the response process. For a change from one equilibrium climate to another, however, climate feedback may be viewed as modifying either the forcing or the response. Thus the cloud feedback parameter $\Delta\text{CRF}/G$, as here defined, refers to a modification of the forcing. Alternatively, a cloud feedback derivative can be defined as $\Delta\text{CRF}/(\lambda G) = \Delta\text{CRF}/\Delta T_s$ so as to refer to a response modification.

Cloud radiative forcing and its solar and infrared components are summarized in Table 12 for the 19 GCM simulations. The agreement is far from good, with the solar and infrared components producing respective variations by factors of 2 and 3. While it might be tempting to include ERBE measurements in Table 12, this has not been done since the present simulations are for a perpetual July, and there is no assurance that this is consistent with a seasonal July.

The climate-induced changes in cloud radiative forcing, and its solar and infrared components, are summarized in Table 13; again, there are considerable variations amongst the models. But an important point is that this summary allows a simple identification and interpretation of cloud

TABLE 13. Differences in Solar, Infrared, and Net Cloud Forcing for the ΔSST = ±2°K Change

Model	ΔCRF, W m^{-2}		
	Solar	Infrared	Net
CCC	−0.9	0.2	−0.7
ECMWF	−5.9	3.0	−2.9
MGO	−0.3	−1.3	−1.6
DNM	2.0	−1.8	0.3
GFDL II	0.1	−0.2	−0.1
DMN	1.8	−0.8	1.0
CSU	3.8	−3.0	0.8
OSU/IAP	0.7	1.6	2.3
OSU/LLNL	−0.4	1.0	0.6
BMRC	4.3	−4.2	0.2
MRI	1.5	0.7	2.1
GFDL I	1.5	0.3	1.8
UKMO	4.4	−3.4	1.0
CCM1	2.6	0.6	3.2
CCM/LLNL	2.1	0.8	2.9
LMD	3.7	1.1	4.8
ECHAM	5.6	−0.8	4.8
CCM0	7.4	−2.3	5.1
GISS	5.1	−0.5	4.6

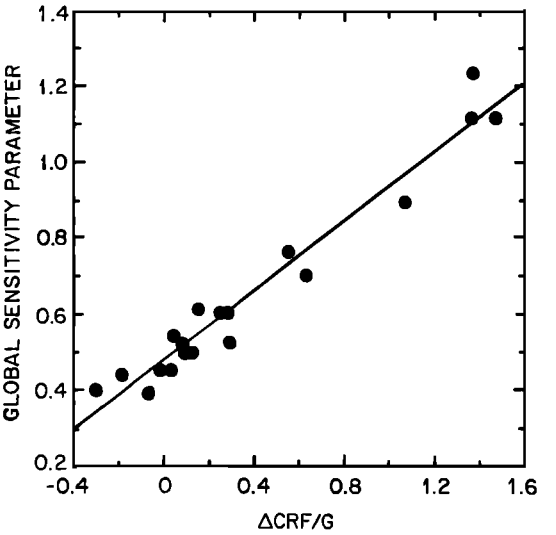

Fig. 2. The global sensitivity parameter λ (K m^2 W^{-1}) plotted against the cloud feedback parameter ΔCRF/G for the 19 GCMs. The solid line represents a best-fit linear regression.

feedback. For example, as discussed in the previous section the CSU and OSU/LLNL GCMs produce comparable climate sensitivity but for quite different reasons. This is consistent with Table 13, which shows that the two models produce similar and modest ΔCRF, although with significantly different solar and infrared components of this quantity. The results of Table 13 are also consistent with our prior elucidation of a negative solar feedback in GFDL II relative to GFDL I due to the former containing cloud albedos that are dependent upon cloud water content. On the other hand, the fact that CCM1 and CCM/LLNL have fairly similar solar ΔCRF values is, as previously discussed, a consequence of near-compensatory albedo and cloud-amount feedbacks in the CCM/LLNL GCM.

A further perspective is given by the λ_c and λ/λ_c summary of Table 14. The excellent agreement of the models' clear-sky sensitivity is again emphasized, while the variations in global sensitivity (Table 9) are attributable primarily to variations in cloud feedback. This ranges from a modest negative feedback for the ECMWF model to strong positive feedback for CCM0.

TABLE 14. Summary of λ_c and λ/λ_c

Model	λ_c, K m^2 W^{-1}	$\lambda/\lambda_c = 1 + \Delta CRF/G$
CCC	0.42	0.93
ECMWF	0.57	0.70
MGO	0.54	0.81
DNM	0.44	1.03
GFDL II	0.46	0.98
DMN	0.44	1.12
CSU	0.46	1.09
OSU/IAP	0.40	1.29
OSU/LLNL	0.48	1.08
BMRC	0.52	1.04
MRI	0.47	1.28
GFDL I	0.48	1.25
UKMO	0.53	1.15
CCM1	0.43	1.63
CCM/LLNL	0.49	1.55
LMD	0.43	2.07
ECHAM	0.47	2.36
CCM0	0.45	2.47
GISS	0.52	2.37

An additional way of illustrating that cloud feedback is the primary cause of the intermodel variations in global climate sensitivity is the scatter plot of Figure 2, which is a plot of λ versus the cloud feedback parameter ΔCRF/G for the 19 GCMs. Here the solid line represents a linear fit to the 19 models as is consistent with (9). Clearly, the intermodel differences in global climate sensitivity are dominated by their corresponding differences in cloud feedback as represented by the parameter ΔCRF/G. Conversely, scatter about the regression line denotes intermodel differences in the clear sensitivity parameter λ_c, and, as previously emphasized, these differences are rather minor. The point of Figure 2 is that it supports the suggestion that cloud-climate feedback is a significant cause of intermodel differences in climate change projections. These differences are, of course, a direct result of the large intermodel range of ΔCRF/G values.

As previously emphasized, the dependence of cloud optical properties upon cloud water content constitutes a potential negative feedback mechanism. However, differentiating between models that do or do not incorporate this effect does not aid in understanding the large differences in cloud feedback as produced by the 19 GCMs. Eight of the models incorporate, at least to some degree, this effect (Tables 3 and 4, the dependence of cloud optical properties upon temperature for the two OSU models is to distinguish between water and ice clouds). These are the CCC, CSU, DMN, ECHAM, ECMWF, LMD, CCM/LLNL and GFDL II models. But when these eight models are distinguished from the other ten, as in Figure 3, there clearly is not a segregation into low- and high-sensitivity groups on the basis of whether they do or do not incorporate cloud optical properties that depend upon cloud water content. Nor is there an obvious sensitivity segregation in terms of other factors, such as models with or without a diurnal cycle, penetrating convection versus moist adiabatic adjustment, or spectral versus finite difference.

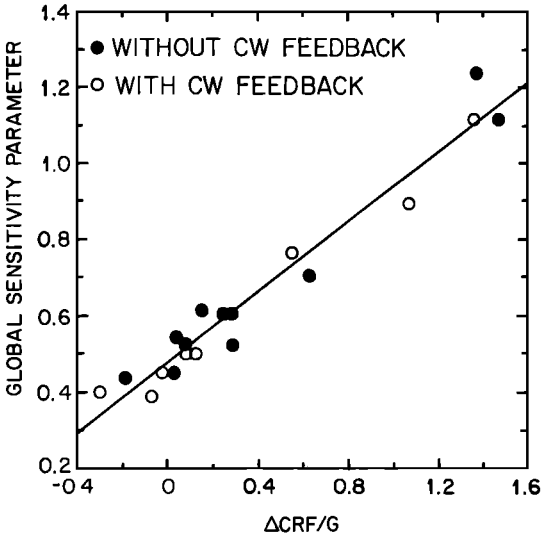

Fig. 3. The same as in Figure 2, but differentiating between models that do not or do incorporate cloud optical properties as a function of cloud water content (CW feedback).

7. Concluding Remarks

The purpose of the present GCM intercomparison has been to focus on global atmospheric feedback processes, with the goal of identifying those processes that are primarily responsible for producing intermodel differences in climate sensitivity. This intercomparison, utilizing perpetual July simulations and adopting SST perturbations as a surrogate climate change, shows that 19 GCMs produce climate sensitivity parameters that differ by roughly a factor of 3. This variability is primarily attributable to differences amongst the models in their depictions of cloud feedback.

While the surrogate climate change adopted within the present study does not provide an estimate of a model's true climate sensitivity, certain of the results are consistent with our understanding of climate sensitivity. For example, following the same approach used in arriving at (4) but adopting $F_c = 270$ W m^{-2}, the clear-sky sensitivity parameter in the absence of interactive feedback mechanisms is

$$\lambda_c = 0.27 \text{ m}^2 \text{ °C W}^{-1} \tag{10}$$

Recall further that the clear-sky sensitivity represents that without cloud feedback, and for this the present set of 19 GCMs yields

$$\lambda_c \simeq 0.47 \text{ m}^2 \text{ °C W}^{-1} \tag{11}$$

The roughly 70% enhancement in sensitivity for (11) versus (10) is, in fact, consistent with the early radiative-convective model study by *Manabe and Wetherald* [1967] and many others since. In that investigation the enhancement was due to water-vapor feedback; i.e., as the climate warms the atmosphere contains more water vapor and that amplifies the warming, since water vapor is itself a greenhouse gas. Recently, *Raval and Ramanathan* [1989] have employed satellite data to quantify this positive feedback, and the present GCM simulations are consistent with this observational study [*Cess*, 1989]. The important point is that the 19 models produce closely comparable and observationally consistent clear-sky sensitivity parameters.

With the inclusion of cloud feedback this compatibility vanishes and there is roughly a threefold variation in climate sensitivity as produced by the models. From Table 14 it is seen that the models' cloud feedback ranges from modest negative to strong positive feedback. Clearly, a first-order priority for future model improvements is the treatment of clouds within GCMs. But it must also be realized that there are many other facets of a GCM, in addition to cloud optical properties and cloud formation parameterizations, that can influence cloud-climate interactions within a model. It should be stressed that cloud feedback must be understood to be the consequence of all interacting physical and dynamical processes in a model when simulating climate change. The result of all these processes is to produce changes in temperature, moisture distribution, and clouds which are integrated into the radiative response termed cloud feedback.

Many GCMs are in a continual state of evolution, and thus the present GCM summary may not represent the latest configuration of a specific model. Furthermore, the model-produced cloud feedbacks found in the present study are probably not representative of how the models would behave under realistic climate change conditions. Perpetual July simulations cannot be used for this, nor can the uniform SST perturbations be used, since they do not incorporate changes in equator-to-pole temperature gradients associated with actual climatic change. For example, it has recently been speculated [*Ramanathan et al.*, 1989] that this latter effect, by itself, may produce a cloud feedback component due to latitudinal shifts in general circulation patterns. But these caveats do not alter the primary conclusion of this study, which is that 19 different GCMs produce a broad spectrum of cloud-climate feedback. There are, of course, other factors that can produce intermodel differences in climate sensitivity when models are used for actual climate change simulations. One such factor, which is not an issue in the present study, refers to differences in model-produced control climates resulting in different climate sensitivities [*Spelman and Manabe*, 1984; *Cess and Potter*, 1988].

On a final point the present study illustrates the fact that climate research benefits from a diversity of climate models. If only one model were available, we could not so confidently conclude that cloud feedback is a key issue for climate dynamics.

Appendix A: Summary of the Modifications to the CCC GCM

The version of the CCC GCM used in this calculation differs substantially from the original version [*Boer et al.*, 1984]. The purpose of this appendix is to summarize these changes.

Instead of prescribed zonal clouds with fixed optical properties, the version used in this study computes fractional cloud cover C based on relative humidity h, as

$$C = \frac{h - h_o}{1 + h_o} \tag{A1}$$

where h_o is a prescribed threshold, which in this particular case is a simple function of temperature.

Cloud optical properties are a function of model temperature via a diagnostic estimation of the liquid water content of the clouds. The cloud liquid water content ℓ is evaluated

from the expression for adiabatic condensation at ambient temperature following *Betts and Harshvardhan* [1987] as

$$\ell = \langle (C_p T/L\theta) \rangle \Gamma_w \Delta p \tag{A2}$$

where

$$\Gamma_w = -\langle \partial\theta/\partial p)_{\theta_{ES}} \rangle \tag{A3}$$

and where θ is the potential temperature and p the pressure. In (A2), Δp is chosen in order to fit observations at various temperatures [*Feigelson*, 1978]. The visible optical depth τ is obtained from

$$\tau = \frac{3}{2R_e(\ell)} \int_{\text{base}}^{\text{top}} \ell \, dz \tag{A4}$$

where the equivalent droplet radius $R_e(\ell)$ is taken from observations. The cloud emissivity is estimated as

$$\varepsilon = 1 - \exp(-3\tau/4) \tag{A5}$$

as suggested by *Platt and Harshvardhan* [1988] based on observations. The visible single scattering albedo of clouds is also parameterized in terms of optical depth with the asymmetry factor for cloud droplets fixed at 0.8511.

Finally, cloud albedo is calculated using the delta-Eddington method. The solar radiation scheme is essentially that described by *Fouquart and Bonnel* [1980], extended to 2 spectral intervals. The scheme for terrestrial radiation calculation has been developed by *Morcrette et al.* [1986]. It includes five long-wave spectral regions. Other changes to the model include: (1) the use of piecewise-constant finite elements in the vertical, (2) hybrid coordinate in the vertical, (3) the use of the transformed variable 1/ln (q) for moisture, (4) improved surface hydrology, (5) minor changes in the moist convection scheme, and (6) a modified gravity-wave drag scheme.

A forthcoming report will document these, and subsequent modifications to the CCC GCM and the resulting reference climate.

Appendix B: Treatment of Cloud Optical Properties in the GFDL II GCM

In the GFDL II GCM the theoretical liquid water content of clouds is assumed to be proportional to the condensed water within the clouds according to

$$W_p = C\Delta r_p \Delta p/g$$

where W_p is vertical water/ice path within the cloud (grams per square meter), Δr_p is the change of water-vapor mixing ratio due either to small-scale or large-scale condensation, Δp is the pressure thickness of the cloud layer, g is gravitational acceleration, and the constant C is determined by calibrating the cloud radiative forcing of the model's standard integration to a preliminary version of the Earth Radiation Budget Experiment (ERBE) for July. This produced $C \simeq 0.5$.

In deriving the relationships between cloud water content and cloud optical properties, the following assumptions were made: (1) The computations were based upon a direct solar beam; (2) A constant solar zenith angle was employed (53°); (3) Mie scattering theory was utilized; and (4) The delta-Eddington approximation was employed for radiative transfer calculations. The drop-size distributions are from *Chýlek and Ramaswamy* [1982] or water clouds and from *Heymsfield* [1975] for ice clouds.

Letting R and A respectively denote the cloud reflectivity and absorptivity for solar radiation, while ε is the infrared cloud emissivity, then for water clouds the above procedure yields

$$R = 0.87(1 - e^{-0.13\delta_1})$$

$$A = 0.13(1 - e^{-0.068\delta_1})$$

$$\varepsilon = 1.0$$

while for ice clouds

$$R = 0.80(1 - e^{-0.13\delta_2})$$

$$A = 0.20(1 - e^{-0.086\delta_2})$$

$$\varepsilon = 1 - e^{-\delta_2}$$

where

$$\delta_1 = 0.24 w_p \qquad \delta_2 = 0.074 w_p$$

The fact that δ_2 describes both A and ε is coincidental.

These expressions were derived and kindly provided by V. Ramaswamy. This scheme for computing cloud optical properties is not incorporated into any operational GFDL GCM, but was used only for this particular study.

Appendix C: Treatment of Clouds and Radiation in the CCM/LLNL GCM

The treatment of solar radiation within the CCM/LLNL GCM is based upon *Wiscombe*'s [1977] delta-Eddington code. The solar spectrum is divided into three wavelength intervals: below 0.4 μm, 0.4–0.9 μm, and beyond 0.9 μm. Water vapor absorption is treated using the exponential sum-fit method of *Somerville et al.* [1974]. The ozone absorption optical depths for the UV and visible bands were determined by matching the absorption of the direct solar beam with the absorptance formulas of *Lacis and Hansen* [1974].

The cloud optical depth is evaluated from the geometric optics expression

$$\tau = \frac{3w\Delta z}{2\rho r_e}$$

where $w\Delta z$ is the liquid water path, ρ is the density of liquid water, and $r_e = 7$ μm is the effective cloud droplet radius [*Charlock and Ramanathan*, 1985]. The single scattering albedo for clouds is unity below 0.9 μm, while beyond 0.9 μm it is 0.99 for stratiform clouds and 0.98 for convective clouds. For all clouds and all wavelengths the asymmetry factor is 0.85.

The treatment of clouds follows *Ramanathan et al.* [1983], except that the cloud liquid water path is diagnosed as the water condensed from each model layer as simulated every 30 min, with the constraint that the liquid water be confined to the overcast fraction of the grid [*Harshvardhan and Randall*, 1985], and with the effect of cloud-scale convective moisture transport accounted for to prevent the diagnosis of

negative liquid water concentrations. Saturation is assumed to occur at 100% relative humidity. For stratiform clouds the fractional cloudiness is 100%; for convective clouds it is 30% with random overlap for infrared radiation and vertical coherence for solar radiation. The dependence of cloud emissivity upon cloud liquid water content is from *Stephens* [1978].

APPENDIX D: MODIFICATIONS TO THE OSU/IAP GCM

In order to produce more realistic distributions of convective clouds within the OSU/IAP GCM, the relaxation time τ_c for the convective adjustment, defined as the *e*-folding time for the instability to be removed, has been modified from the assumed value of 1 hour [*Zeng et al.*, 1989]. In this modification, τ_c is assumed to have the latitudinal distribution

$$\tau_c(\text{hour}) = \frac{1.25}{0.25 + |\sin \phi|}$$

where ϕ is latitude.

Acknowledgments. We appreciate the valuable insights and suggestions that have been provided by M. E. Schlesinger. This GCM intercomparison project was performed under the auspices of the Atmospheric and Climate Research Division, U.S. Department of Energy, under grant DEFG0285-ER60314 to SUNY Stony Brook, contract W-7405-ENG-48 to Lawrence Livermore National Laboratory, and contract DE-AI01-80EV10220 to the National Center for Atmospheric Research, which is sponsored by the National Science Foundation. Further support was provided by NASA's Climate Program under grant NAG 5-1058 to Colorado State University, by the Bundesminister für Forschung und Technologie, F.R.G., through grant KF20128 to the University of Hamburg, and by the Commission of European Communities through contract EV4C-0066-F to DMN/CNRM. Computing resources were also provided to Colorado State University by the Numerical Aerodynamic Simulation Program at NASA Ames Research Center.

REFERENCES

Alexander, R. C., and R. L. Mobley, Monthly average sea-surface temperatures and ice-pack limits on a 1° global grid, *Mon. Weather Rev.*, *104*, 143–148, 1976.

Arakawa, A., and V. R. Lamb, Computational design of the basic dynamical processes of the UCLA general circulation model, *Methods Comput. Phys.*, *17*, 173–265, 1977.

Betts, A. K., and Harshvardhan, Thermodynamic constraint on the cloud liquid water feedback in climate models, *J. Geophys. Res.*, *92*, 8483–8485, 1987.

Boer, G. J., N. A. McFarlane, R. Laprise, J. D. Henderson, and J.-P. Blanchet, The Canadian Climate Centre spectral atmospheric general circulation model, *Atmos. Ocean*, *22*, 297–429, 1984.

Cariolle, D., A. Lasserre-Bigorry, J. F. Royer, and J. F. Geleyn, A GCM simulation of the springtime Antarctic ozone decrease and its impact on mid-latitudes, *J. Geophys. Res.*, *95*, 1883–1898, 1990.

Cess, R. D., Climatic change: An appraisal of atmospheric feedback processes employing zonal climatology, *J. Atmos. Sci.*, *33*, 1831–1843, 1976.

Cess, R. D., Gauging water-vapour feedback, *Nature*, *342*, 736–737, 1989.

Cess, R. D., and G. L. Potter, Exploratory studies of cloud radiative forcing with a general circulation model, *Tellus*, *39A*, 460–473, 1987.

Cess, R. D., and G. L. Potter, A methodology for understanding and intercomparing atmospheric climate feedback processes in general circulation models, *J. Geophys. Res.*, *93*, 8305–8314, 1988.

Cess, R. D., and I. L. Vulis, Intercomparison and interpretation of satellite-derived directional albedos over deserts, *J. Climate*, *2*, 393–407, 1989.

Cess, R. D., G. L. Potter, S. J. Ghan, and W. L. Gates, The climatic effects of large injections of atmospheric smoke and dust: A study of climate feedback mechanisms with one- and three-dimensional climate models, *J. Geophys. Res.*, *90*, 12,937–12,950, 1985.

Cess, R. D., et al., Interpretation of cloud-climate feedback as produced by 14 atmospheric general circulation models, *Science*, *245*, 513–516, 1989.

Charlock, T. P., and V. Ramanathan, The albedo field and cloud radiative forcing produced by a general circulation model with internally generated cloud optics, *J. Atmos. Sci.*, *42*, 1408–1429, 1985.

Chýlek, P., and V. Ramaswamy, Simple approximation for infrared emissivity of water clouds, *J. Atmos. Sci.*, *39*, 171–177, 1982.

Coiffier, J., Y. Ernie, J. F. Geleyn, J. Clochard, J. Hoffman, and F. Dupont, The operational hemispheric model at the French Meteorological Service, *J. Meteorol. Soc. Jpn.*, Spec. NWP Symp. Vol., 337–345, 1987.

Feigelson, E. M., Preliminary radiation model of a cloudy atmosphere, 1, Structure of clouds, and solar radiation, *Beitr. Phys.*, *51*, 203–229, 1978.

Fouquart, Y., and B. Bonnel, Computation of solar heating of the Earth's atmosphere: A new parameterization, *Beitr. Phys.*, *53*, 35–62, 1980.

Ghan, S. J., J. W. Lingaas, M. E. Schlesinger, R. L. Mobley, and W. L. Gates, A documentation of the OSU two-level atmospheric general circulation model, *Rep. 61*, 391 pp., Climatic Res. Inst., Oreg. State Univ., Corvallis, 1982.

Hansen, J., G. Russell, D. Rind, P. Stone, A. Lacis, S. Lebedeff, R. Ruedy, and L. Travis, Efficient three-dimensional global models for climate studies: Models I and II, *Mon. Weather Rev.*, *111*, 609–662, 1983.

Hansen, J., A. Lacis, D. Rind, G. Russel, P. Stone, I. Fung, and J. Lerner, Climate sensitivity: Analysis of feedback mechanisms, in *Climate Processes and Climate Sensitivity*, *Geophys. Monogr. Ser.*, vol. 29, pp. 130–163, AGU, Washington, D. C., 1984.

Harshvardhan, and D. A. Randall, Comments on "The parameterization of radiation for numerical weather prediction models," *Mon. Weather Rev.*, *113*, 1832–1833, 1985.

Hart, T. L., W. Bourke, B. J. McAvaney, B. W. Forgan, and J. L. McGregor, Atmospheric general circulation simulations with the BMRC global spectral model: The impact of revised physical parameterizations, *J. Climate*, *3*, 436–459, 1990.

Heymsfield, A., Cirrus uncinus generating cells and the evolution of cirriform clouds, Part I, Aircraft observations of the growth of the ice phase, *J. Atmos. Sci.*, *32*, 799–808, 1975.

Lacis, A. A., and J. E. Hansen, A parameterization for the absorption of solar radiation in the Earth's atmosphere, *J. Atmos. Sci.*, *31*, 118–133, 1974.

Le Treut, H., and Z.-X. Li, Using Meteosat data to validate a prognostic cloud generation scheme, *Atmos. Res.*, *21*, 273–292, 1988.

Manabe, S., and R. T. Wetherald, Thermal equilibrium of the atmosphere with a given distribution of relative humidity, *J. Atmos. Sci.*, *24*, 241–259, 1967.

Marchuk, G., V. Dymnikov, V. Zalesny, V. Lykosov, and V. Galin, *Mathematical Modeling of General Circulation of the Atmosphere*, Springer-Verlag, New York, 1986.

McClatchey, R. A., R. W. Fenn, J. E. A. Selby, F. E. Volz, and J. S. Garing, Optical properties of the atmosphere, *Rep. AFCRL-71-0279*, 85 pp., Air Force Cambridge Res. Lab., Cambridge, Mass., 1971.

Mitchell, J. F. B., C. A. Senior, and W. J. Ingram, CO_2 and climate: A missing feedback?, *Nature*, *341*, 132–134, 1989.

Morcrette, J.-J., Radiation and cloud radiative properties in the ECMWF operational weather forecast model, *J. Geophys. Res.*, in press, 1990.

Morcrette, J.-J., L. Smith, and Y. Fouquart, Pressure and temperature dependence of the absorption in longwave radiation parameterization, *Beitr. Phys.*, *59*, 455–469, 1986.

Petukhov, V. K., Ye. M. Feygelson, and N. I. Manuylova, The regulating role of clouds in the heat effects of anthropogenic aerosols and carbon dioxide, *Izv. Atmos. Oceanic Phys.*, *11*, 802–809, 1975.

Platt, C. M. R., and Harshvardhan, Temperature dependence of

cirrus extinction: Implications for climate feedback, *J. Geophys. Res.*, *93*, 11,051–11,058, 1988.

Ramanathan, V., The role of Earth radiation budget studies in climate and general circulation research, *J. Geophys. Res.*, *92*, 4075–4095, 1987.

Ramanathan, V., E. J. Pitcher, R. C. Malone, and M. Blackmon, The response of a general circulation model to refinements in radiative processes, *J. Atmos. Sci.*, *40*, 605–630, 1983.

Ramanathan, V., R. D. Cess, E. F. Harrison, P. Minnis, B. R. Barkstrom, E. Ahmad, and D. Hartmann, Cloud-radiative forcing and climate: Results from the Earth radiation budget experiment, *Science*, *243*, 57–63, 1989.

Randall, D. A., Harshvardhan, D. A. Dazlich, and T. Corsetti, Interactions among radiation, convection, and large-scale dynamics in a general circulation model, *J. Atmos. Sci.*, *46*, 1944–1970, 1989.

Raval, A., and V. Ramanathan, Observational determination of the greenhouse effect, *Nature*, *342*, 758–761, 1989.

Sadourny, R., and K. Laval, January and July performance of the LMD GCM, in *New Perspectives in Climate Modelling*, edited by A. Berger and C. Nicolis, Elsevier, New York, 1984.

Schlesinger, M. E., and J. F. B. Mitchell, Model projections of the equilibrium climatic response to increased CO_2, *Rev. Geophys.*, *89*, 760–798, 1987.

Slingo, A. (Ed.), Handbook of the Meteorological Office 11-layer atmospheric general circulation model, *Rep. DCTN*, *29*, Meteorol. Off., Bracknell, U. K., 1985.

Slingo, J. M., The development and verification of a cloud prediction scheme for the ECMWF model, *Q. J. R. Meteorol. Soc.*, *113*, 899–927, 1987.

Sokolov, A. P., January atmospheric circulation simulated by a global spectral model, *Meteorol. Hydrol.*, *2*, 12–21, 1986.

Somerville, R. C. J., and L. A. Remer, Cloud optical thickness feedbacks in the CO_2 climate problem, *J. Geophys. Res.*, *89*, 9668–9672, 1984.

Somerville, R. C. J., et al., The GISS model of the global atmosphere, *J. Atmos. Sci.*, *31*, 84–117, 1974.

Spelman, M. J., and S. Manabe, Influence of oceanic heat transport upon the sensitivity of a model climate, *J. Geophys. Res.*, *89*, 571–586, 1984.

Stephens, G. L., Radiation profiles in extended water clouds, II, Parameterization schemes, *J. Atmos. Sci.*, *35*, 2123–2132, 1978.

Suarez, J. J., A. Arakawa, and D. A. Randall, Parameterization of the planetary boundary layer in the UCLA general circulation model: Formulation and results, *Mon. Weather Rev.*, *111*, 2224–2243, 1983.

Tokioka, T., K. Yamazaki, I. Yagai, and A. Kitoh, A description of the Meteorological Research Institute atmospheric general circulation model (MRI GCM-I), *Tech. Rep. 13*, 249 pp., Meteorol. Res. Inst., Tsukuba, Japan, 1984.

Washington, W. M., and G. A. Meehl, Seasonal cycle experiment on the climate sensitivity due to a doubling of CO_2 with an atmospheric general circulation model coupled to a simple mixed-layer ocean model, *J. Geophys. Res.*, *89*, 9475–9503, 1984.

Wetherald, R. T., and S. Manabe, The effects of changing the solar constant on the climate of a general circulation model, *J. Atmos. Sci.*, *32*, 2044–2059, 1975.

Wetherald, R. T., and S. Manabe, Cloud feedback processes in a general circulation model, *J. Atmos. Sci.*, *45*, 1397–1415, 1988.

Williamson, D. L., J. T. Kiehl, V. Ramanathan, R. E. Dickinson, and J. J. Hack, Description of NCAR Community Climate Model (CCM1), *Tech. Note TN-285+STR*, Natl. Cent. for Atmos. Res., Boulder, Colo., 1987.

Wilson, C. A., and J. F. B. Mitchell, A $2 \times CO_2$ climate sensitivity experiment with a global climate model including a simple ocean, *J. Geophys. Res.*, *92*, 13,315–13,343, 1987.

Wiscombe, W. J., The delta-Eddington approximation for a vertically inhomogeneous atmosphere, *Tech. Note TN-121+STR*, 30 pp., Natl. Cent. for Atmos. Res., Boulder, Colo., 1977.

Zeng, Q.-C., X.-H. Zhang, X.-Z. Liang, C.-G. Yuan, and S.-F. Chen, Documentation of the IAP Two-Level Atmospheric General Circulation Model, *Rep. ER/60314-H1*, 383 pp., Dep. of Ener., Washington, D. C., 1989.

J. P. Blanchet and G. J. Boer, Canadian Climate Centre, Atmospheric Environment Service, Department of the Environment, 4905 Dufferin St., Downsview, Ontario M3H 5T4, Canada.

R. D. Cess, Institute for Terrestrial and Planetary Atmospheres, State University of New York, Stony Brook, NY 11794.

A. D. Del Genio and A. A. Lacis, NASA Goddard Institute for Space Studies, 2880 Broadway, New York, NY 10025.

M. Déqué and J. F. Royer, Direction de la Météorologie, CNRM, 42 Avenue, Coriolis 31057 Toulouse Cédex, France.

V. Dymnikov and V. Galin, Department of Numerical Mathematics, USSR Academy of Sciences, 29 Ryleeva Street, Moscow 119034, USSR.

W. L. Gates, S. J. Ghan, G. L. Potter, and K. E. Taylor, Lawrence Livermore National Laboratory, P. O. Box 808, L-264, Livermore, CA 94550.

J. T. Kiehl, A. Slingo, and W. Washington, National Center for Atmospheric Research, P. O. Box 3000, Boulder, CO 80307.

H. Le Treut and Z.-X. Li, Laboratoire de Météorologie Dynamique, 24 Rue Lhomond, 75231 Paris Cédex 05, France.

X.-Z. Liang, and M.-H. Zhang, Institute of Atmospheric Physics, Beijing, China.

B. J. McAvaney and L. Rikus, Bureau of Meteorology Research Centre, GPO Box 1289K, Melbourne, 3001 Victoria, Australia.

V. P. Meleshko, D. A. Sheinin, and A. S. Sokolov, Voeikov Main Geophysical Observatory, 7 Karbisheva, Leningrad 194018, USSR.

J. F. B. Mitchell, Meteorological Office (Met 0 20), London Road, Bracknell, Berkshire RG12 2SZ, England.

J.-J. Morcrette, European Centre for Medium-Range Weather Forecasts, Reading, Berkshire RG2 9AX, England.

D. Randall, Department of Atmospheric Sciences, Colorado State University, Fort Collins, CO 80523.

E. Roeckner and V. Schlese, Meteorologisches Institut, University of Hamburg, Bundesstrasse 55, D 2000, Hamburg 13, Federal Republic of Germany.

R. T. Wetherald, Princeton University, NOAA/GFDL, P. O. Box 308, Princeton, NJ 08540.

I. Yagai, Meteorological Research Institute, 1-1 Nagamine, Tsukuba, Ibaraki-ken 305, Japan.

(Received December 19, 1989;
revised April 11, 1990;
accepted May 14, 1990.)